Heat Mass Transfer (2008) 44:1391–1399
DOI 10.1007/s00231-008-0377-5

ORIGINAL

Finite Péclet number forced convection past a sphere in a porous medium using a thermal nonequilibrium model

Hilda H. Y. Kwan · D. Andrew S. Rees · Ioan Pop

Received: 20 September 2007 / Accepted: 23 January 2008 / Published online: 12 February 2008

Abstract We study the finite-Péclet number forced convective heat transfer from a uniform temperature sphere placed in otherwise uniform fluid stream within a porous medium. A numerical study is undertaken to determine how the lack of local thermal equilibrium between the phases affects temperature fields of the two phases and the respective rates of heat transfer from the sphere. On the upstream side of the sphere the temperature field extends further from the sphere in the solid phase than it does for the fluid phase, but the opposite is true on the downstream side.

List of symbols

a	radius of sphere (m)
c	specific heat (kJ kg^{-1} K^{-1})
h	solid/fluid heat transfer coefficient (W m^{-3} K^{-1})
H	nondimensional solid/fluid heat transfer coefficient
k	thermal conductivity (W m^{-1} K^{-1})
K	permeability of the porous medium (m^2)
LTE	local thermal equilibrium
LTNE	local thermal nonequilibrium
Nu	local rate of heat transfer
$\overline{Nu}$	global rate of heat transfer
$\bar{p}$	pressure (kg m^{-1} s^{-2})
Pe	Péclet number
r	radial coordinate (m)
T	dimensional temperature (K)
u	Darcy velocity in the r-direction (m s^{-1})
U	dimensional free stream velocity (m s^{-1})
v	Darcy velocity in the α-direction (m s^{-1})

Greek symbols

α	angular coordinate
γ	modified conductivity ratio
μ	fluid viscosity (kg m^{-1} s^{-1})
ρ	fluid density (kg m^{-3})
θ	temperature of fluid phase
ϕ	temperature of solid phase
ψ	streamfunction

Subscripts

h	surface of the sphere
f	fluid phase
s	solid phase
∞	ambient condition

Superscript

$-$	dimensional variable

H. H. Y. Kwan · D. A. S. Rees (✉)
Department of Mechanical Engineering,
University of Bath, Claverton Down, Bath BA2 7AY, UK
e-mail: ensdasr@bath.ac.uk

D. A. S. Rees
Department of Mathematics, University of Bristol,
University Walk, Bristol BS8 1TW, UK

I. Pop
Faculty of Mathematics, University of Cluj, 3400 Cluj,
CP253, Romania

1 Introduction

Heat transfer in porous media is an important phenomenon in a variety of practical engineering applications. These include the utilisation of geothermal energy, the control of pollutant spread in groundwater, the insulation of buildings, solar power collectors, design of nuclear reactors and

compact heat exchangers, to name but a few. A comprehensive literature survey on this subject can be found in the recent books by Ingham and Pop [1–3], Nield and Bejan [6], Vafai [16, 17] and Pop and Ingham [7].

Very little work has been undertaken on forced convection past a hot sphere embedded in a porous medium, unlike the analogous case of convection past a hot cylinder, and the literature is represented by the papers by Romero [12, 13], Sano [14] and Pop and Yan [8]. Romero [12] has shown that, for high Péclet number forced convection past a sphere, we may obtain solutions for a wide variety of boundary conditions. In particular we can obtain analytical approximations for a sphere with a prescribed heat flux, or with a prescribed but spatially varying temperature distribution on its surface. This work was extended to a prolate spheroid in [13]. The paper by Sano [14] uses the method of matched asymptotic expansions to find solutions in term of the Péclet number. Pop and Yan [8], on the other hand, show that it is possible to find a similarity solution for the thermal field in the large-Péclet limit.

However, all the above-quoted solutions for forced convection past a sphere in a porous medium assume the condition of local thermal equilibrium (LTE) between the fluid and the solid porous matrix. By this is meant that the fluid and solid phases are taken to have the same temperature locally over lengthscales which are small compared with the radius of the sphere but which are big relative to the detailed microstructure of the porous medium; see Nield and Bejan [6]. However, in applications using porous media, such as the environmental impact of buried nuclear heat-generating waste, chemical reactors, thermal energy transport/storage systems and the cooling of electronic devices, a temperature discrepancy between the solid matrix and the saturating fluid has been observed and recognised. Therefore an analysis of separate energy equations for the two phases, that is, a local non-equilibrium model, has assumed increasing importance. Further references on this topic may be found in the recent papers by Wong et al. [18] and Rees et al. [10], which are concerned with the analogous problem of forced convection about a circular cylinder, and in the reviews by Kuznetsov [5] and Rees and Pop [11].

2 Formulation of the problem

A steady flow takes place past a hot sphere of radius a, which is embedded in a porous medium of ambient temperature T_∞. We shall assume that the uniform free stream velocity is U and that the temperature of the sphere is T_h where $T_h > T_\infty$, although there is no reason why the sphere should not be colder than the oncoming stream. An axisymmetric spherical–polar coordinate system, (r,α) is chosen, with the origin at the centre of the sphere. The $\alpha = 0$ axis is taken to be in the direction of the free stream and we are able to assume axisymmetry. Our main aim is to determine the heat transfer characteristics of this system, and how they are altered by the presence of local thermal nonequilibrium. On taking the Darcy flow model, the equations describing the steady forced convection flow may be written as,

$$\frac{\partial}{\partial \bar{r}}\left(\bar{r}^2 \bar{u}\sin\alpha\right) + \frac{\partial}{\partial \alpha}\left(\bar{r}\bar{v}\sin\alpha\right) = 0, \tag{1a}$$

$$\bar{u} = -\frac{K}{\mu}\frac{\partial \bar{p}}{\bar{r}}, \tag{1b}$$

$$\bar{v} = -\frac{K}{\mu}\frac{1}{\bar{r}}\frac{\partial \bar{p}}{\partial \alpha}, \tag{1c}$$

$$\epsilon k_f \bar{\nabla}^2 T_f = (\rho c)_f \left(\bar{u}\frac{\partial T_f}{\partial \bar{r}} + \frac{\bar{v}}{\bar{r}}\frac{\partial T_f}{\partial \alpha}\right) + h(T_f - T_s), \tag{1d}$$

$$(1-\epsilon)k_s \bar{\nabla}^2 T_s = h(T_s - T_f), \tag{1e}$$

where

$$\bar{\nabla}^2 = \frac{1}{\bar{r}^2}\left[\frac{\partial}{\partial \bar{r}}\left(\bar{r}^2\frac{\partial}{\partial \bar{r}}\right) + \frac{1}{\sin\alpha}\frac{\partial}{\partial \alpha}\left(\sin\alpha\frac{\partial}{\partial \alpha}\right)\right] \tag{2}$$

is the Laplacian operator in axisymmetric spherical polar coordinates. The quantities $\bar{u}$ and $\bar{v}$ denote the fluid velocities in the radial and transverse directions, $\bar{r}$ and α, respectively, while T is the temperature, $\bar{p}$ the pressure, K the permeability, μ the fluid viscosity, k the conductivity, ρ the density, c the specific heat, and ε the porosity. The subscripts f and s denote fluid and solid, respectively.

It is important to note that the coefficient, h, is used to model the microscale transfer of heat between the fluid and the solid phases. The value of h depends not only on the conductivities of the solid and fluid phases, but also on the porosity, the detailed geometry of the porous medium and on the microscopic Reynolds number; for more details see Kuznetsov [5], Rees and Pop [11] and Rees [9].

The equations of motion may now be nondimensionalised using the transformations,

$$\bar{r} = ar, \quad (\bar{u},\bar{v}) = U(u,v), \tag{3a}$$

$$T_f = (T_c - T_\infty)\theta + T_\infty, \quad T_s = (T_c - T_\infty)\phi + T_\infty, \tag{3b}$$

where θ and ϕ are the temperatures of the fluid and solid phases, respectively. In addition we also introduce the nondimensional streamfunction, ψ, according to

$$u = \frac{1}{r^2\sin\alpha}\frac{\partial \psi}{\partial \alpha}, \quad v = -\frac{1}{r\sin\alpha}\frac{\partial \psi}{\partial r}. \tag{4}$$

After the elimination of the pressure terms in Eqs. (1b,1c), we obtain,

$$\frac{\partial^2\psi}{\partial r^2}+\frac{1}{r^2}\left(\frac{\partial^2\psi}{\partial\alpha^2}-\cot\alpha\frac{\partial\psi}{\partial\alpha}\right)=0, \tag{5a}$$

$$Pe^{-1}\nabla^2\theta+H(\phi-\theta)=\frac{1}{r^2\sin\alpha}\left(\frac{\partial\psi}{\partial\alpha}\frac{\partial\theta}{\partial r}-\frac{\partial\psi}{\partial r}\frac{\partial\theta}{\partial\alpha}\right), \tag{5b}$$

$$Pe^{-1}\nabla^2\phi+H\gamma(\theta-\phi)=0. \tag{5c}$$

Here ∇^2 is the nondimensional form of the Laplacian, $\bar{\nabla}^2$, given in (2), and the constants,

$$H=\frac{ah}{U(\rho c)_f},\quad \gamma=\frac{\epsilon k_f}{(1-\epsilon)k_s},\quad \text{and}\quad Pe=\frac{Ua(\rho c)_f}{\epsilon k_f}, \tag{6}$$

are a nondimensional inter-phase heat transfer coefficient, a porosity-scaled conductivity ratio and the Péclet number, respectively. Equations (5a, b, c) are to be solved subject to the boundary conditions,

$$\begin{aligned}&\psi=0,\quad \theta=\phi=1\quad \text{on}\quad r=1,\\ &\psi\to\frac{1}{2}r^2\sin^2\alpha,\quad \theta,\phi\to\quad \text{as}\quad r\to\infty.\end{aligned} \tag{7}$$

Equation (5a) subject to (7) may be solved readily to obtain,

$$\psi=\frac{1}{2}\left(r^2-\frac{1}{r}\right)\sin^2\alpha, \tag{8}$$

which may be shown easily to give the appropriate form for the uniform free stream when r is large. Substituting (8) into Eqs. (5b, c) gives

$$\begin{aligned}&Pe^{-1}\left[\frac{\partial^2\theta}{\partial r^2}+\frac{2}{r}\frac{\partial\theta}{\partial r}+\frac{1}{r^2}\left(\frac{\partial^2\theta}{\partial\alpha^2}+\cot\alpha\frac{\partial\theta}{\partial\alpha}\right)\right]\\ &\quad=\left(1-\frac{1}{r^3}\right)\cos\alpha\frac{\partial\theta}{\partial r}-\left(\frac{1}{r}+\frac{1}{2r^4}\right)\sin\alpha\frac{\partial\theta}{\partial\alpha}+H(\theta-\phi),\end{aligned} \tag{9a}$$

$$Pe^{-1}\left[\frac{\partial^2\phi}{\partial r^2}+\frac{2}{r}\frac{\partial\phi}{\partial r}+\frac{1}{r^2}\left(\frac{\partial^2\phi}{\partial\alpha^2}+\cot\alpha\frac{\partial\phi}{\partial\alpha}\right)\right]=H\gamma(\phi-\theta). \tag{9b}$$

We are particularly interested in how the isotherm patterns of the fluid and solid phases differ from one another, and how they contribute towards local and global rates of heat transfer. The local rates of heat transfer per unit area are given by

$$Nu_f=-\left.\frac{\partial\theta}{\partial r}\right|_{r=1},\quad Nu_s=-\left.\frac{\partial\phi}{\partial r}\right|_{r=1}, \tag{10}$$

while the global rates of heat transfer per unit area are given by

$$\overline{Nu}_f=-\frac{1}{2}\int_0^\pi\left.\frac{\partial\theta}{\partial r}\right|_{r=1}\sin\alpha d\alpha \tag{11a}$$

and

$$\overline{Nu}_s=-\frac{1}{2}\int_0^\pi\left.\frac{\partial\phi}{\partial r}\right|_{r=1}\sin\alpha d\alpha. \tag{11b}$$

3 Numerical method

The coupled equations for the temperatures of the fluid and solid phases, Eqs. (7), were solved using second order accurate central difference approximations. When the Péclet number is large, systems like (9a, b) require substantial under-relaxation in order to obtain convergence and we employed an unsteady method. These equations were supplemented by adding first order time-derivatives to the right hand sides of Eq. (9a, b). We employed the DuFort–Frankel method for time stepping, details of which may be found in many textbooks, such as that of Smith [15].

Given that the line $\alpha=0,\ \pi$ is a line of symmetry we confined our computations to half of the physical domain, and the correct symmetry was assured by setting the first α-derivative of both θ and ϕ to zero at $\alpha=0$ and π.

The external boundary, which is located at a suitably large value of r, is both an inflow and an outflow boundary. In the range $\frac{1}{2}\pi<\alpha<\pi$ fluid flows into the computational domain and therefore we set $\theta=\phi=0$ on that part of the boundary. However, fluid flows out in the range $0\le\alpha<\frac{1}{2}\pi$ and therefore it is more difficult to choose a good boundary condition. While it is possible to use a very large value of r as the radius of the computational domain in order to eliminate upstream effects of a poor outflow condition, this iscomputationally expensive. As in [18], two different methods were used: (1) setting the second r-derivative to zero, and (2) adopting a buffer region methodology. The ideabehind the first method is to allow the temperature fields as much freedom as possible to evolve, but it was not found to behave uniformly well. Quite often pointwise spatial oscillations arose near outflow, thereby degrading the integrity of the solution. Often these oscillations were coupled with a lack of convergence to the steady state. The second method is drawn from recent work on the simulation of boundary layer instabilities where disturbances to the basic flow are artifically damped out by multiplying the disturbance field by an appropriate function (which is equal to 1 over most of the computational domain, but which decreases smoothly to 0 at the outflow boundary); see Kloker et al. [4] for a detailed discussion of this topic. While the buffer region method was designed for following boundary layer instabilities, we found that it also works extremely well in the present context. By its very nature, the buffer region does modify the temperature field locally near outflow, but it has negligible upstream effect. In fact there is little difference in the results obtained between methods (1) and (2) except for near the outflow boundary.

However it was found that method (2) was much more robust.

During the preliminary stages of our numerical work, we found that the distance the thermal field penetrates from the sphere into the surrounding porous medium depends strongly on the values of Pe and H, and therefore the maximum radius we used in the simulations also needed to vary quite considerably. For large values of both Pe and H the value $r_{\max} = 3$ was found to be sufficient, but when when Pe and H are both relatively small $r_{\max}$ was sometimes greater than 100. This latter case reflects the fact that conduction has a relatively strong effect in both phases when Pe is small and more so in the solid phase when H is small. In almost all cases the number grid points in the α-direction was taken to be 160. The size of the timestep is of no consequence since the aim is to determine the resulting steady-state thermal fields as efficiently as possible.

4 Numerical solutions

The solutions to the governing equations (9a, b), depend on the the three independent parameters Pe, H and γ. We shall present solutions firstly in the form of detailed isotherms in order to display how the thermal fields vary with changes in the parameters, and then both the local and the global rates of heat transfer are presented.

In Figs. 1, 2, 3 and 4 detailed isotherms are shown, where the flow, which is given by Eq. (8), proceeds from left to right. In these figures the fluid-phase isotherms are displayed in the upper half, while those for the solid phase are displayed in the lower half.

Figure 1 compares the thicknesses of the thermal regions of the two phases for a selection of values of the Péclet number when $H = \gamma = 1$. These values of H and γ are such that local thermal nonequilibrium (LTNE) effects are moderate. The chief difference between the small and the large values of Pe lies in the thickness of the boundary layers, but in all four cases shown the thermal field within the solid phase is more extensive on the upstream side of the sphere than is the field in the fluid phase. Although θ and ϕ are coupled, there is no advection term in the ϕ equation which allows ϕ to diffuse further upstream than θ. For small values of Pe is small, conduction effects are generally more significant than advection, at least near the sphere, and therefore both temperature fields extend a large distance from the sphere. But as Pe increases, advection becomes increasingly dominant. A thermal boundary forms on the upstream side of the sphere accompanied by increasing rates of heat transfer. When $Pe = 1{,}000$ a well-defined boundary layer has formed most of the way around the sphere, and grows substantially.

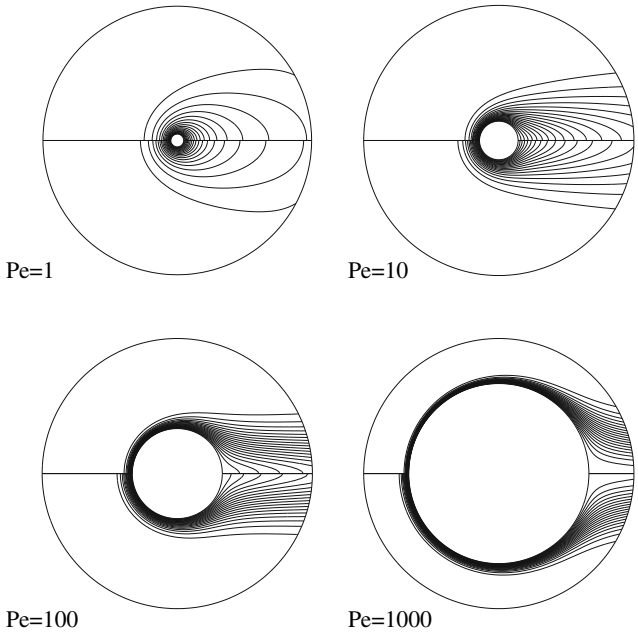

Fig. 1 Isotherm plots for forced convection past a uniform temperature sphere with $H = \gamma = 1$. Isotherms for the fluid phase occupy the upper half of each subfigure while the lower half corresponds to the solid phase. Isotherms are plotted at intervals of 0.05; this convention also applies to Figs. 2, 3 and 4. The values of the Péclet number are, 1, 10, 100, 1,000

The effect of variations in H on the isotherms are shown in Fig. 2 where we have taken $Pe = 100$ and $\gamma = 1$. This figure shows the changes in the ease with which heat is transferred between the phases. When $H = 0.01$ the spatial extent of the thermal field in the solid phase is substantially greater than within the fluid phase. At this value of H very little heat is passed to the solid phase which allows for strong conductive effects. When H increases more heat is transferred between the phases which causes the thermal field of the solid phase to shrink quite rapidly. Conversely there is slight, barely noticeable shrinking in the thermal field of the fluid phase. There remains a slight mismatch between the isotherms of the respective phases on the axis when $H = 10$, but this has disappeared when $H = 100$.

Figure 3 shows the $Pe = 1$ counterpart to the cases shown in Fig. 2. The strength of the external flow is now 1% of that corresponding to Fig. 2 and therefore the thermal fields of both phases are much more extensive. Once more we see that the solid phase isotherms extend considerably further than those of the fluid phase when H is small, and that the thermal fields become identical when H becomes large.

Figure 4 shows the effect of changing γ when $Pe = 100$ and $H = 1$. Firstly we note that large values of γ cause the temperature of the solid phase to react quickly to changes in the temperature of the fluid phase, and therefore we recover LTE in the large-γ limit even though $H = 1$. Indeed, it may

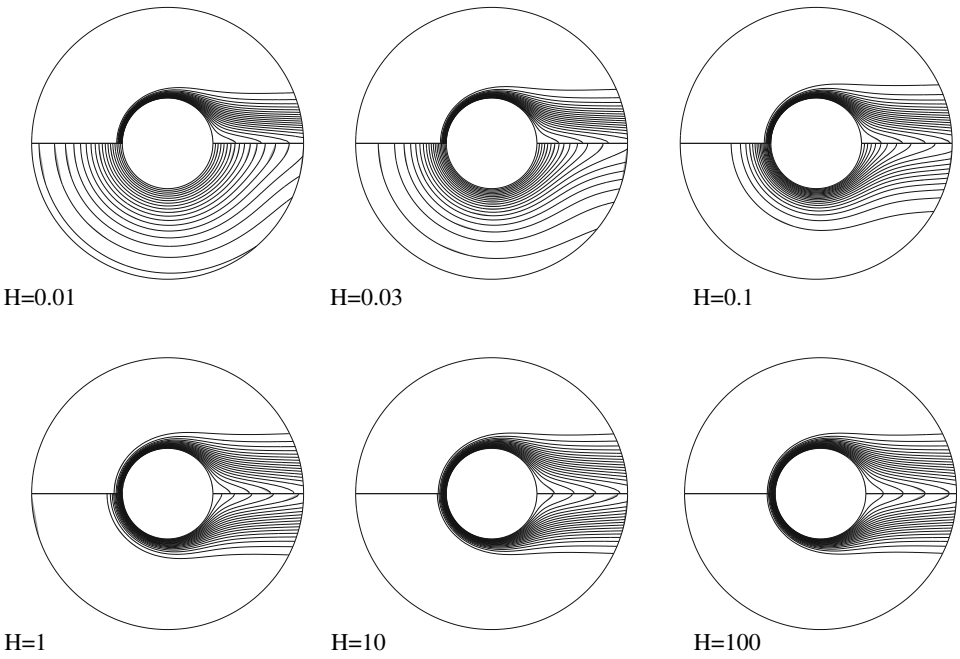

Fig. 2 The effect of different values of H on the isotherms for $Pe = 100$ and $\gamma = 1$. The parameter H takes the values 0.01, 0.03, 0.1, 1, 10 and 100

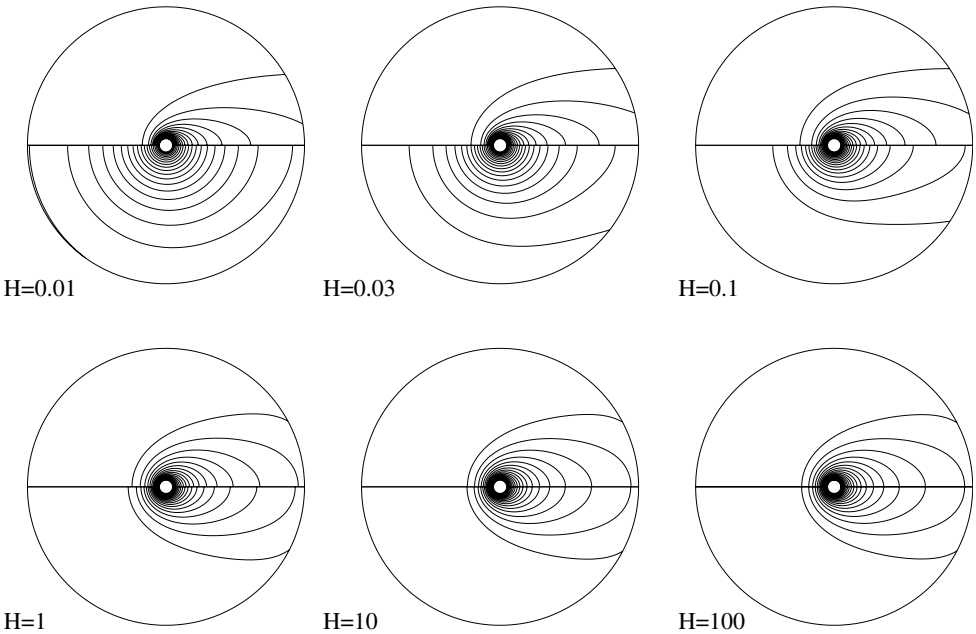

Fig. 3 The effect of different values of H on the isotherms for $Pe = 1$ and $\gamma = 1$. The parameter H takes the values 0.01, 0.03, 0.1, 1, 10 and 100

be shown that $\theta - \phi = O(\gamma^{-1})$ when γ is large. On the other hand, when γ reduces in size, the thermal fields of both phases increase substantially in size. Given that γ multiplies the source/sink term in the equation for ϕ, the temperature of the solid phase almost independent of the fluid phase when $\gamma = 1$, and therefore thermal field of the solid phase becomes large. However, the source/sink term in the equation for θ is still significant, which means that the fluid depends quite strongly on the behaviour of the solid phase. In particular, this means that the thermal field of the fluid phase is also large when γ is small.

Figures 5, 6, 7 and 8 show local rates of heat transfer which correspond to the isotherm plots displayed in Figs. 1, 2, 3 and 4, respectively. All these figures show that the local rate of heat transfer increases monotonically from $\alpha = 0$, the rear stagnation point, to $\alpha = \pi$, the forward stagnation point. At the rear stagnation point the thermal boundary layer lifts off the sphere, and the rate of heat transfer is particularly small there. On the other hand, at the forward stagnation point a relatively large rate of heat transfer occurs as the fluid flow opposes conduction. Figure 5, in particular, shows that the rate of heat transfer is

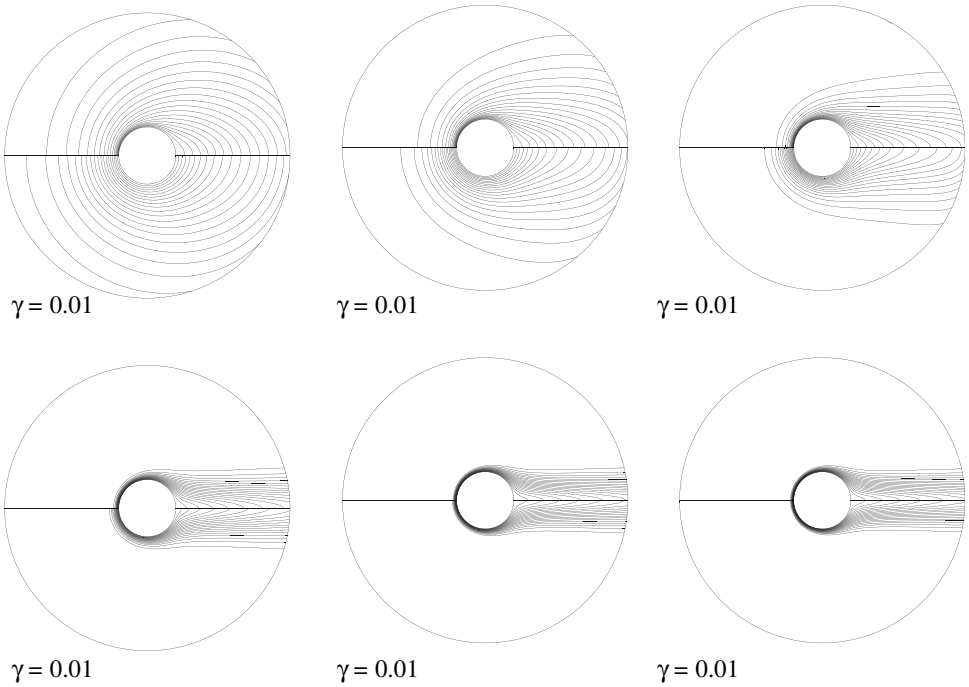

Fig. 4 The effect of different values of γ on the isotherms for $Pe = 100$ and $H = 1$. The parameter γ takes the values 0.01, 0.03, 0.1, 1, 10 and 100

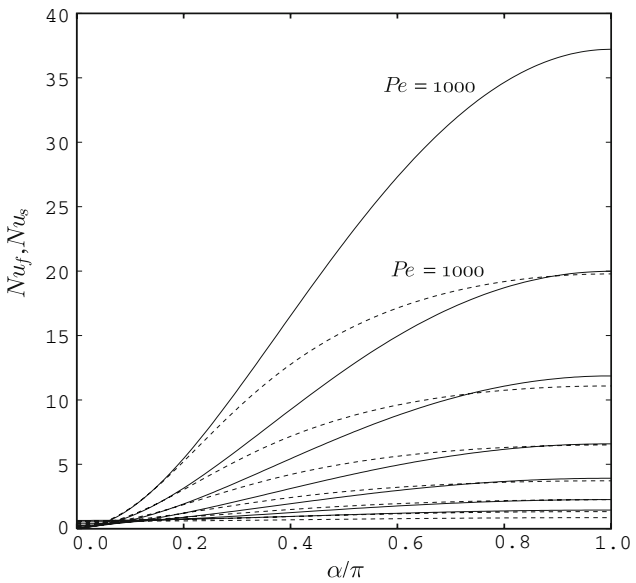

Fig. 5 Values of Nu_f (*continuous lines*) and Nu_s (*dashed lines*) as functions of α for $H = \gamma = 1$ and $Pe = 1$, 3, 10, 30, 100, 300 and 1000. At $\alpha = \pi$ both Nu_f and Nu_s increase with Pe

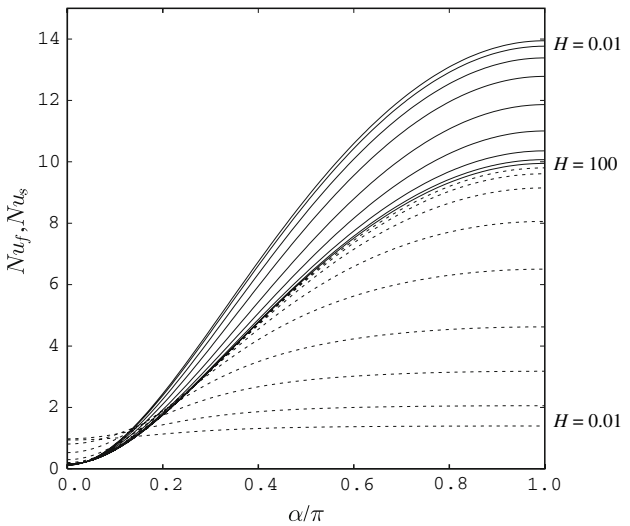

Fig. 6 Values of Nu_f (*continuous lines*) and Nu_s (*dashed lines*) as functions of α for $Pe = 100$ and $\gamma = 1$ with $H = 0.01$, 0.03, 0.1, 0.3, 1, 3, 10, 30 and 100. At $\alpha = \pi$ both Nu_f and Nu_s vary monotonically with H

relatively large and becomes increasingly so as the Péclet increases, and the thermal fields tend towards boundary layer form. On the other hand, when $H = 0.01$ in Fig. 6, we see clearly the strong decoupling the fluid and solid phases. The Nu_f curve shows a substantial variation which is typical in such forced convective situation. However, the Nu_s curve is alomst constant, which shows that the thermal field of the solid phase is almost indepdent of the flow, and that conduction effects dominate.

A simple examination of Figs. 6 and 7 shows that, in all cases, the local heat transfer of the fluid phase is higher than that of the solid phase over most of the sphere and including the upstream stagnation point. This happens because conduction is assisted by advection within the fluid phase. However, close to the rear stagnation point, the situation is not as simple, for the solid phase exhibits the higher rate of heat transfer when $Pe = 100$, but exhibits the lower rate of heat transfer when $Pe = 1$. At higher values of the Péclet number the strength of the flow causes

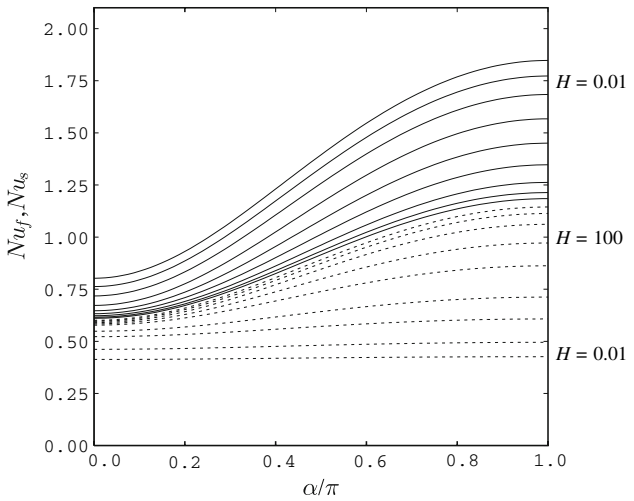

Fig. 7 Values of Nu_f (*continuous lines*) and Nu_s (*dashed lines*) as functions of α for $Pe = 1$ and $\gamma = 1$ with $H = 0.01$, 0.03, 0.1, 0.3, 1, 3, 10, 30 and 100. At $\alpha = \pi$ both Nu_f and Nu_s vary monotonically with H

the thermal field to lift away from the cylinder over a small region close to the rear stagnation point, which yields the relatively low rate of heat transfer there. But when Péclet takes smaller values, the thermal fields are much thicker, and the fact that the fluid phase has the higher rate of heat transfer follows simply from the fact the the thermal field in the fluid phase is a little more compressed than its solid phase counterpart.

Similar comments apply when we consider variations in γ, as shown in Fig. 8. Small values of γ cause Nu_s to vary only slightly with position around the sphere, while the opposite is true when γ is large.

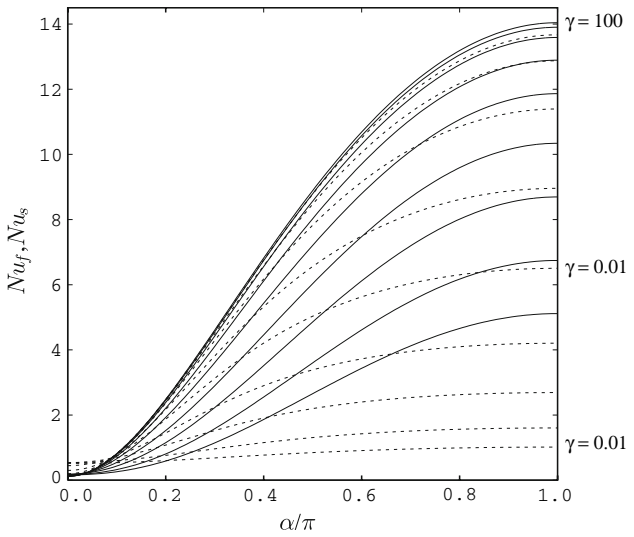

Fig. 8 Values of Nu_f (*continuous lines*) and Nu_s (*dashed lines*) as functions of α for $Pe = 100$ and $H = 1$ with $\gamma = 0.01$,0.03, 0.1, 0.3, 1, 3, 10, 30 and 100. At $\alpha = \pi$ both Nu_f and Nu_s increase with γ

Finally, we consider some detailed values of the global rates of heat transfer. The numbers displayed in each Table have errors which are much less than 1%; higher accuracy can be obtained by either using a much finer grid, which will take considerably more CPU time, or by using more sophisticated methods.

Table 1 shows how the global rates of heat transfer vary with H when $H = \gamma = 1$; these values correspond to the data displayed in Fig. 1. The increase in the rate of heat transfer with Pe is very evident, and we note that there is an approximately tenfold increase in both $\overline{Nu}_f$ and $\overline{Nu}_s$ as Pe increases from 10 to 1,000. This is consistent with the boundary layer analysis of [8] where the local and global rates of heat transfer were found to be proportional to $Pe^{1/2}$ when Pe is large. This is shown more clearly in the last two columns of Table 1 which show how $\overline{Nu}_f/Pe^{1/2}$ and $\overline{Nu}_s/Pe^{1/2}$ vary. It is clear that these quantities are tending towards a well-defined limit.

Tables 2 and 3 show the variations of $\overline{Nu}_f$ and $\overline{Nu}_s$ with H when $\gamma = 1$ and when $Pe = 100$ and $Pe = 1$, respectively, corresponding to the isotherms shown in Figs. 2 and 3. We have already seen that LTE is established as H increases, and these Tables show that the ratio $\overline{Nu}_f/\overline{Nu}_s \to 1$ in the large-H limit. As in [18], it is also necessary to state that the degree of LTNE not only decreases when H increases for fixed values of Pe, but also as Pe decreases when H is fixed. The latter case arises because the increasing dominanation of conduction as the primary mechanism of heat transfer from the sphere gives the phases much more space in which to evolve to the same local values. In mathematical terms, the effect of advection near the surface is now of $O(Pe)$ relative to conduction, and therefore the Eqs. (9a) and (9b) are identical at leading order in Pe.

Finally, Table 4 shows the effect of varying γ when $Pe = 100$ and $H = 1$. As previously noted, the primary effect of small values of γ is to caused the thermal fields of both phases to expand relative to when γ is large, and therefore the associated global rates of heat transfer decrease as γ decreases. It may also be seen that LTNE also

Table 1 Values of $\overline{Nu}_f$ and $\overline{Nu}_s$ as a function of Pe when $H = \gamma = 1$

Pe	$\overline{Nu}_f$	$\overline{Nu}_s$	$\overline{Nu}_f/Pe^{1/2}$	$\overline{Nu}_s/Pe^{1/2}$
1	1.0710	0.7330		
3	1.4822	1.0322		
10	2.3810	1.6412		
30	3.8822	2.6412	0.7088	0.4822
100	6.8468	4.5571	0.6847	0.4557
300	11.5934	7.7355	0.6693	0.4466
1,000	21.1136	13.7550	0.6676	0.4350

Table 2 Values of $\overline{Nu}_f$ and $\overline{Nu}_s$ as a function of H when $Pe = 100$ and $\gamma = 1$

H	$\overline{Nu}_f$	$\overline{Nu}_s$	$\overline{Nu}_f/\overline{Nu}_s$
0.01	8.2797	1.3076	6.3318
0.03	8.1485	1.8445	4.4176
0.1	7.3670	2.6698	2.9522
0.3	7.4401	3.5764	2.0804
1	6.8468	4.5571	1.5024
3	6.3683	5.2188	1.2203
10	6.0546	5.6120	1.0789
30	5.9281	5.7632	1.0286
100	5.8762	5.8240	1.0090

Table 3 Values of $\overline{Nu}_f$ and $\overline{Nu}_s$ as a function of H when $Pe = 1$ and $\gamma = 1$

H	$\overline{Nu}_f$	$\overline{Nu}_s$	$\overline{Nu}_f/\overline{Nu}_s$
0.01	1.3718	0.4203	3.2637
0.03	1.3107	0.4802	2.7298
0.1	1.2388	0.5693	2.1762
0.3	1.5101	0.6385	1.8011
1	1.0703	0.7325	1.4612
3	1.0053	0.7918	1.2697
10	0.9553	0.8391	1.1385
30	0.9266	0.8672	1.0684
100	0.9092	0.8848	1.0276

Table 4 Values of $\overline{Nu}_f$ and $\overline{Nu}_s$ as a function of γ when $Pe = 100$ and $H = 1$

γ	$\overline{Nu}_f$	$\overline{Nu}_s$	$\overline{Nu}_f/\overline{Nu}_s$
0.01	2.6392	0.8212	3.2140
0.03	3.5444	1.2349	2.8701
0.1	4.7172	2.0234	2.3314
0.3	5.7911	3.0786	1.8811
1	6.8468	4.5571	1.5024
3	7.5765	5.9697	1.2692
10	8.0582	7.2075	1.1180
30	8.2655	7.8804	1.0489
100	8.3542	8.2181	1.0166

becomes stronger in that limit, which suggests that thermal conduction in the solid phases becomes significant.

5 Conclusions

In this paper we have examined the steady forced convection boundary layer flow past a hot sphere which is embedded in a fluid-saturated porous medium where a two-temperature model of the microscopic heat transfer between the solid and fluid phases has been adopted. Detailed results for a representative sets of parameters has been presented in a variety of forms: isotherm plots, variation of local rates of heat transfer, and values of global rates of heat transfer.

We find that large values of the Péclet number yield thermal fields that are of boundary layer type, and which should therefore be amenable to a boundary layer analysis. Even within this regime, moderate values of H and γ give rise to LTNE so that the thermal fields within the solid and fluid phases are not identical. Indeed, we find that LTE arises either when H is sufficiently large, or when γ is sufficiently large, even when Pe takes moderate values.

At small values of Pe the thermal field of both phases spreads a considerable distance from the sphere, and it is hoped to be able to perform a small-Pe analysis of this situation in the future.

In general the local rate of heat transfer decreases with distance around the sphere from the upstream stagnation point. Within a boundary layer theory this might be understood easily in terms of the increasing thickness of the boundary layer.

Acknowledgments This paper was completed while the second author (DASR) was enjoying study leave at the University of Bristol. He is grateful to his hosts in the Department of Mathematics for their hospitality.

References

1. Ingham DB, Pop I (eds) (1998) Transport phenomena in porous media, vol 1. Pergamon Press, Oxford
2. Ingham DB, Pop I (eds) (2002) Transport phenomena in porous media, vol 2. Pergamon Press, Oxford
3. Ingham DB, Pop I (eds) (2005) Transport phenomena in porous media, vol 3. Pergamon Press, Oxford
4. Kloker M, Konzelmann U, Fasel H (1993) Outflow boundary conditions for spatial Navier–Stokes simulations of transitional boundary-layers. AIAA J 31:620–628
5. Kuznetsov AV (1998) Thermal nonequilibrium forced convection in porous media. In: Ingham DB, Pop I (eds) Transport phenomena in porous media, vol 1. Pergamon Press, Oxford, pp 103–129
6. Nield DA, Bejan A (2006) Convection in porous media, 3rd edn. Springer, New York
7. Pop I, Ingham DB (2001) Convective heat transfer: mathematical and computational modelling of viscous fluids and porous media. Pergamon Press, Oxford
8. Pop I, Yan B (1998) Forced convection flow past a cylinder and a sphere in a Darcian fluid at large Péclet numbers. Int Commun Heat Mass Transfer 25:261–267
9. Rees DAS (2008) Microscopic modelling of the two-temperature model for conduction in heterogeneous media. J Porous Media (submitted)
10. Rees DAS, Bassom AP, Pop I (2003) Forced convection past a heated cylinder in a porous medium using a thermal nonequilibium model: boundary layer theory. Eur J Mech B Fluids 22:473–486

11. Rees DAS, Pop I (2005) Local thermal nonequilibrium in porous medium convection. In: Ingham DB, Pop I (eds) Transport phenomena in porous media, vol 3. Pergamon Press, Oxford, pp 147–173
12. Romero LA (1994) Low or high Péclet number flow past a sphere in a saturated porous medium. SIAM J Appl Math 54:42–71
13. Romero LA (1995) Low or high Péclet number flow past a prolate spheroid in a saturated porous medium. SIAM J Appl Math 55:952–974
14. Sano T (1996) Unsteady forced and natural convection around a sphere immersed in a porous medium. J Eng Math 30:515–525
15. Smith GD (1978) Numerical solution of partial differential equations: finite difference methods, 2nd edn. O.U.P., Oxford
16. Vafai K (ed) (2000) Handbook of porous media, vol I, Marcel Dekker, New York
17. Vafai K (ed) (2005) Handbook of porous media, vol II. Marcel Dekker, New York
18. Wong WS, Rees DAS, Pop I (2004) Forced convection past a heated cylinder in a porous medium using a thermal nonequilibrium model: finite Péclet number effects. Int J Thermal Sci 43:213–220